Ultramicroscopy 127 (2013) 109–113

Contents lists available at SciVerse ScienceDirect

Ultramicroscopy

journal homepage: www.elsevier.com/locate/ultramic

Characterization of surface metallic states in $SrTiO_3$ by means of aberration corrected electron microscopy

G. Sánchez-Santolino [a,b], J. Tornos [a], F.Y. Bruno [a], F.A. Cuellar [a], C. Leon [a], J. Santamaría [a], S.J Pennycook [b], M. Varela [b,a,*]

[a] GFMC, Departamento. Física Aplicada III, Universidad Complutense de Madrid, 28040 Madrid, Spain
[b] Materials Science and Technology Division, Oak Ridge National Laboratory, Oak Ridge, TN 37831-6071, USA

ARTICLE INFO

Available online 27 July 2012

Keywords:
Scanning transmission electron microscopy
Electron energy loss spectroscopy
Complex oxides
Irradiation damage
2D electron gas

ABSTRACT

An unusual conducting surface state can be produced in $SrTiO_3$ substrates by irradiation with Argon ions from a plasma source, at low energy and high doses. The effects of irradiation are analyzed here by atomic force microscopy (AFM) and aberration corrected scanning transmission electron microscopy (STEM) combined with electron energy loss spectroscopy (EELS). Depth sensitive studies demonstrate the existence of a heavily damaged surface layer and an oxygen vacancy rich layer immediately underneath, both induced during the irradiation process. We find a clear dependence of the Ti oxidation state with the depth, with a very intense Ti^{3+} component near the surface. Oxygen vacancies act as n-type doping by releasing electrons into the lattice and producing an insulator-to-metal transition, which explains the unusual metallic behavior of these samples.

Published by Elsevier B.V.

1. Introduction

Complex oxide materials pose an exciting promise towards the design of electronic devices that could overcome some of the limitations of Si. $SrTiO_3$ (STO) is one of the most widely studied materials for oxide electronics. It has a perovskite structure and an indirect band gap of 3.25 eV which makes it a band insulator. Furthermore, the electronic properties of STO can be easily modulated by doping it with electrons. This can be achieved through substituting La for Sr cations or Nb for Ti atoms, and also by generating O vacancies. These processes introduce n-type mobile carriers in the STO lattice and reduce some Ti atoms to Ti^{+3}, resulting in a mixed valence system [1–3]. N-doping is also responsible for the reported two-dimensional electron gas at the $LaAlO_3/SrTiO_3$ interface [4]. This exciting discovery has increased the interest in this material even more [5–10] and the explanation of the 2D conductivity remains a subject of controversy.

Recent studies have reported that a 2D surface electron gas can be induced in commercial STO single crystals by Ar plasma irradiation [11]. This type of irradiation can produce a metallic state with confined 2D transport properties, presumably resulting from the oxygen vacancies generated by ion beam etching [12–16]. In order to understand the microscopic origin of such metallic layers, we have studied STO substrates etched using an Ar ion milling reactor. We have employed advanced microscopy techniques sensitive to both the surface and also to the bulk, such as atomic force microscopy (AFM) and high resolution scanning transmission microscopy (STEM). These techniques allow the observation of the superficial damage caused by the reactive ion etching (RIE) treatment. Simultaneous high resolution high angle annular dark field (HAADF) and electron energy loss spectroscopy (EELS) images allow the mapping of the oxidation state of Ti, along with the quantification of oxygen concentration.

2. Experimental

Commercial STO single crystals (001) were chemically etched and annealed to ensure a TiO_2 termination [17]. These samples were irradiated with an Ar^+ plasma with RF powers between 20 and 40 W for time periods of 5 min. Electrical transport measurements were obtained with the Van der Paw method [18], using evaporated Al contacts. IV curves were recorded to ensure their Ohmic behavior. AFM images were acquired in a Bruker multimode Nanoscope III A, equipped with 1 μm, 15 μm and 150 μm maximum scanning area scanners. Aberration-corrected STEM HAADF and bright field (BF) imaging and EELS were acquired using a Nion UltraSTEM [19] operated at 100 kV and equipped with a Nion aberration corrector and a Gatan Enfina spectrometer. For spectrum imaging, the electron beam is scanned along the region of interest and an EEL spectrum is acquired in every

* Correspondence to: Oak Ridge National Laboratory, P.O. Box 2008, BLDG 4515, MS 6071, Oak Ridge, TN 37831, USA. Tel.: +1 865 5746387; fax: +1 865 5746098.
E-mail address: mvarela@ornl.gov (M. Varela).

0304-3991/$ - see front matter Published by Elsevier B.V.
http://dx.doi.org/10.1016/j.ultramic.2012.07.013

pixel, along with the ADF signal. The specimens were prepared by conventional mechanical grinding and polishing and Ar ion milling.

3. Results

The samples become conducting after irradiation with RF powers above 25 W. Fig. 1 shows the temperature dependence of the zero-field sheet resistance of samples irradiated with RF powers between 30 and 40 W. These substrates are metallic in the whole measurement range. The resistance decreases as the RF power increases, denoting an enhancement of irradiation damage. A power law AT^2 behavior characteristic of electron–electron interaction [20] is also found below the STO structural transition [21] at 105 K.

AFM was used to study the surface of the treated samples in order to characterize the erosion of the STO single crystals surface. Before irradiation, well defined, atomically flat terraces can be seen (Fig. 2(a)). The terraces have an average width close to 100 nm. Ar irradiation causes severe surface damage. Images in Fig. 2(b,c,d) show the erosion of the surface caused by the irradiation process for different RF powers (20 W, 36 W and 40 W respectively). For the lowest RF powers, terraces are still observed although their edges are somewhat ragged. Increasing the RF power results in loss of surface features and enhanced structural damage. For the most damaged samples the terrace structure is lost completely. Incidentally, a gradual change of the samples aspect is observed: the color of the samples varies from transparent to gray as damage increases.

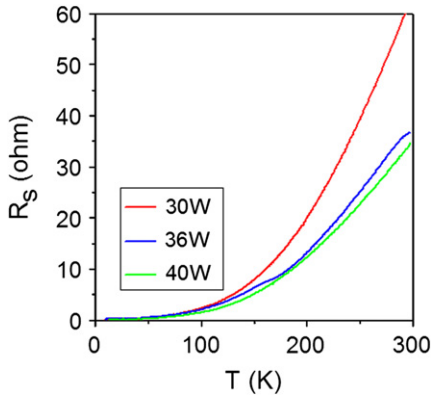

Fig. 1. Temperature dependence of the sheet resistance of crystals irradiated at RF powers from 30 to 40 W for 5 min.

The effects of irradiation can be appreciated in cross-sectional transmission electron microscopy images. Fig. 3 shows simultaneous HAADF and BF images of a sample which was treated in the RIE system at 36 W for 5 min. A damaged surface layer is clearly observed. The images in Figs. 3(a) and (b) show that this damaged layer is continuous and homogeneous over long lateral distances of the order of a few microns. The surface region of the samples exhibits poor crystal quality, voids and amorphous areas, down to a depth of 12 nm. Such loss of crystalline order can also be appreciated in the BF image in Fig. 3(d), which is equivalent to conventional high resolution microscopy. Estimated values of the projected damage range [22,23] of a few nanometers were obtained for the typical 100–200 eV energy range of the irradiation experiments, consistent with the microscopy observations.

In order to assess the effects of the damage on the electronic properties of the samples EELS data were acquired. Line-scans were produced by scanning the electron beam along a line perpendicular to the surface while an EEL spectrum is measured in each pixel. The raw spectra were treated with principal component analysis (PCA) [24] to reduce random noise from spectroscopic images. In order to obtain the oxidation state of titanium and study the oxygen concentration profiles the fine structures of Ti $L_{2,3}$ and O K edges were analyzed. According to the dipole selection rule, the Ti $L_{2,3}$ edge of the transition metals results from the excitation of $2p$ electrons to unoccupied states of $3d$ nature. These edges show two characteristic white lines, originated from transitions from the $2p_{3/2}$ (L_3) and $2p_{1/2}$ (L_2) levels (split by the spin–orbit interaction) to empty levels of the $3d$ band. The Ti L_2 and L_3 lines are further split in two, as observed by x-ray absorption [25] and EELS [26], due to the crystal-field splitting of the threefold t_{2g} (d_{xy}, d_{yz} and d_{xz} orbitals) and twofold e_g ($3d_{z^2-r^2}$ and $3d_{x^2-y^2}$ orbitals) states. The L_3 first peak shows

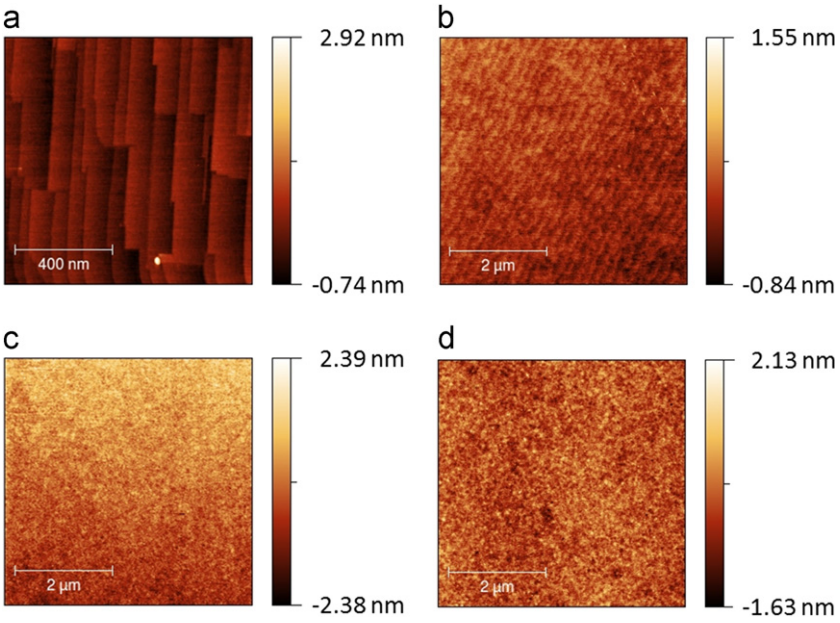

Fig. 2. AFM images of samples irradiated at different energies: no irradiation (a), 20 W (b), 36 W (c) and 40 W (d).

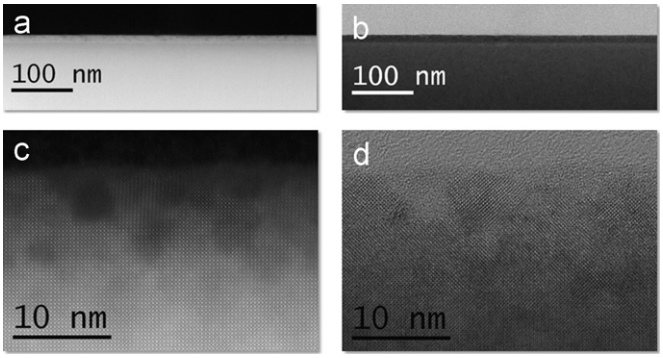

Fig. 3. STEM images of a sample irradiated at 36 W for 5 min. Low magnification HAADF (a) and BF (b) images along with high magnification HAADF (c) and BF (d) images.

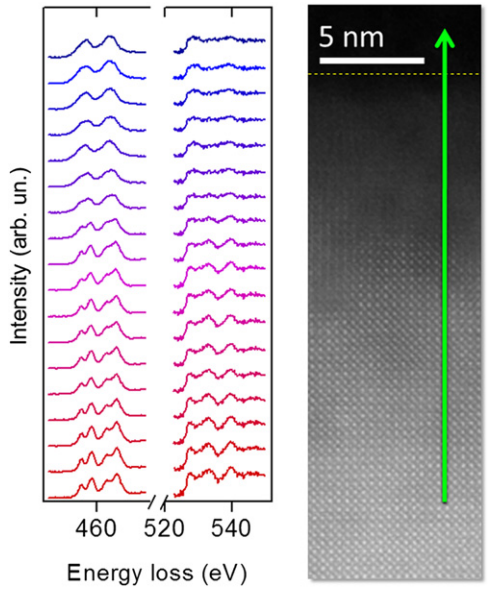

Fig. 4. EEL spectra of Ti $L_{2,3}$ and O K edges obtained along the arrow marked in the HAADF image with an exposure time of 1 s/pixel of a sample irradiated at 36 W for 5 min. The EELS intensity has been normalized in order to show clearly the variation of the peaks along the spectrum image, and the spectra have been shifted vertically for clarity. A dotted line on the HAADF image marks the position of the surface.

transitions from the $2p_{3/2}$ Ti level to the t_{2g} level, and the L_2 first peak, from $2p_{1/2}$ to the e_g level. This splitting is strongly affected by changes in the occupation of the Ti 3d band. On the other hand, the O K edge (around 530 eV), gives us information on excitations of oxygen 1s electrons to 2p bands, which are hybridized with empty Ti 3d orbitals [27]. The near edge fine structure suffers significant changes with the occupancy of 3d states in Ti and therefore it also provides information about the Ti oxidation state. This edge shows two peaks at the onset around 530 eV, due to Ti 3d t_{2g}-e_g splitting and is highly sensitive to bonding features [28]. Hence, the analysis of the O K edge pre-peak will also provide information about the Ti 3d band occupancy and its oxidation state. O K spectra show another set of bands around 537–546 eV. These bands originate from interactions between oxygen 2p states, and Ti 4s and 4p states [29].

In Fig. 4, we show the variation of Ti $L_{2,3}$ and O K edges when the electron beam is placed on the surface and scanned into the material. The Ti $L_{2,3}$ edge away from the surface shows features typical of the bulk Ti^{+4}, with a noticeable crystal field splitting. But closer to the surface it looks more like a Ti^{+3} state, where only two peaks can be seen. The $L_{2,3}$ onset also exhibits a chemical shift and moves to lower energies near the surface. These changes are consistent with a decrease in the oxidation state of Ti atoms [30], although some smearing of the fine structure due to amorphization may be possible. The 3d orbital, unoccupied in the bulk ($3d^0$), would become partially filled in the surface ($3d^1$) as Ti changes from a $+4$ to a $+3$ oxidation state. This Ti oxidation state can be quantified through the analysis of the Ti $L_{2,3}$ edge. In order to do so, a method based on the spatial-difference technique [31] has been used: a multiple linear least-squares fit (MLLS) to the reference spectra of $LaTiO_3$ (Ti^{+3}) and $SrTiO_3$ (Ti^{+4}) from reference [32] is performed. The fit coefficients give the statistical weights associated with the Ti^{+3} and Ti^{+4} components, providing a way to map the Ti valence. Fig. 5 shows another line-scan from the same sample, with the O K and Ti $L_{2,3}$ edges (Fig. 5(b)). For this data set, Fig. 5(c) shows the result of this analysis (in red). The topmost surface layer, heavily damaged, exhibits a drastically reduced Ti, with oxidation states near $+3$. As the electron beam moves into the material, a more bulk-like Ti valence is recovered, about 10 nm into the substrate. The average value for the Ti oxidation state below the damaged layer is $+3.89 \pm 0.11$ (red dotted line in Fig. 5(c)). This value is maintained as deep into the substrate as the whole measurement range, tens of nanometers.

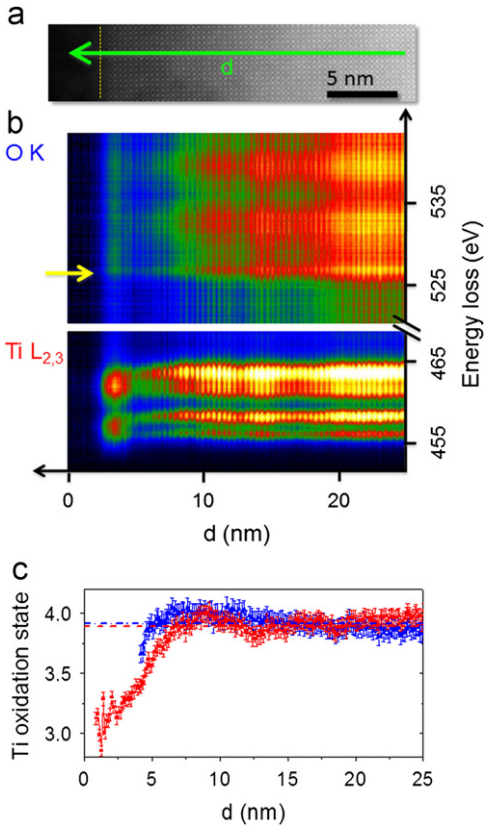

Fig. 5. EELS line-scan along with Ti oxidation state quantification of the sample irradiated at 36 W for 5 min. The simultaneously acquired Ti $L_{2,3}$ and O K edges are shown. The intensities of both edges show a dip 3–4 nm from the surface, most likely due to inhomogeneities in specimen thickness due to the ion mill process: (a) HAADF image showing the direction of the scan (green arrow). The surface is marked with a yellow dashed line. (b) EELS data, showing the O K and the Ti $L_{2,3}$ edges acquired with an exposure time of 1 s/pixel. A yellow arrow marks the onset (pre-peak feature) of the O K edge. (c) Ti oxidation state profiles along the direction of the green arrow in (a), on a matching scale: the oxidation state profile calculated from the O K (Ti $L_{2,3}$) edge is shown in blue (red). (For interpretation of the references to color in this figure, the reader is referred to the web version of this article.)

The value of the Ti oxidation state can also be extracted from the analysis of the O *K* edge, where a clear evolution can also be seen. The edge onset shifts to higher energy losses near the surface (the onset is marked with a yellow arrow on Fig. 5(b)), characteristic of a reduction of the Ti valence state [30]. The separation between the first and the second peak decreases significantly, as the intensity of the pre-peak is also reduced. A way to quantify these changes consists of measuring the difference in peak positions between the pre-peak and the adjacent main peak (ΔE) of the oxygen *K* edge [24,32]. Gaussian curves are fitted to both the pre-peak and the main peak, and the difference in positions for the centers of both Gaussians is extracted along the line spectra shown in Fig. 5. Assuming that there is a linear correlation between the ΔE and Ti oxidation state [31] and using the values of ΔE from bulk STO (ΔE=3,73 eV) and LTO (ΔE=5,61 eV) thick film as a reference [32], the Ti oxidation state can be extracted. However, since the O *K* fine structure is so smeared out near the surface the method renders artifacts for the first few atomic layers, so these points have not been included here. For the rest of the scan, the quantification is reliable and is shown in blue in Fig. 5(c). We obtain a +3.6 oxidation state near the surface. Again, within a length scale of 10 nm the Ti oxidation state increases and reaches a value of $+3.92 \pm 0.06$.

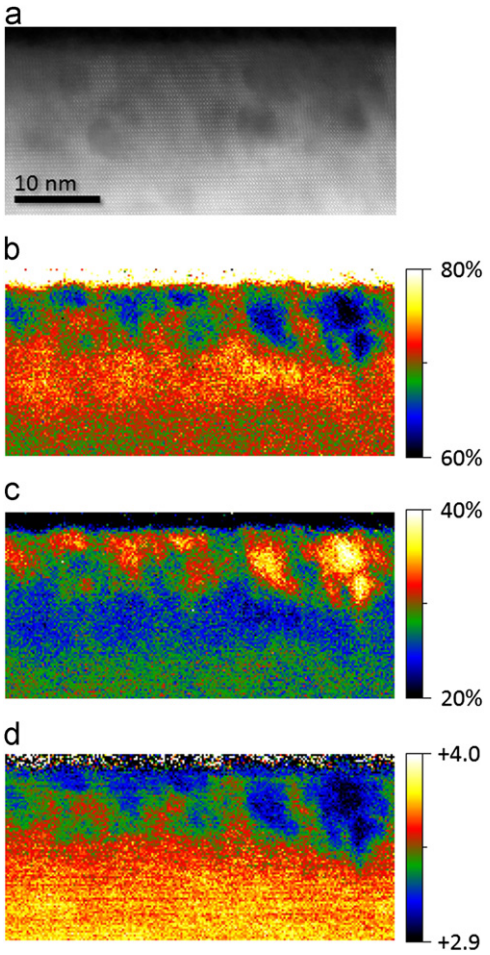

Fig. 6. EELS spectrum-image along with relative compositional maps and Ti oxidation state quantification of a sample irradiated at 36 W for 5 min: (a) HAADF image of the damaged surface area acquired simultaneously with the spectrum image. Relative compositional maps for oxygen (b) and titanium (c) obtained from the quantification of the O *K* and Ti $L_{2,3}$ edges, respectively. (d) Ti oxidation state map obtained with the MLLS method applying to the Ti $L_{2,3}$ edge. The dark blue zones correspond to Ti^{+3} state and the light yellow zones are close to Ti^{+4} state. On the dark blobs the residual of the MLLS fit is large enough (2–4%) that some presence of Ti^{+2} cannot be ruled out. The top few pixels correspond in all cases to the glue line. These pixels have been ignored for quantification purposes. (For interpretation of the references to color in this figure, the reader is referred to the web version of this article.)

The values obtained from both methods employed agree well within error bars, and they clearly denote a mixed distribution of Ti^{+3} and Ti^{+4} in the heavily damaged layer near the surface. As we go deeper in the material, the concentration of Ti^{+4} increases but the oxidation state does not reach +4 completely within the measurement range. Unfortunately, in our experiments we are limited to surface studies: the specimen thickness increases as we move deeper into the material preventing high quality EELS data acquisition. The estimated thickness of the confinement zone suggested by magnetotransport data is 260 nm [11], a depth range that can hardly be probed in our STEM specimens. Nevertheless, two distinct regimes near the surface layer are observed, so in order to gain lateral statistics 2D spectrum images were acquired. Fig. 6(a) shows a high resolution HAADF image of the damaged surface area. Heavily damaged zones, where the crystalline contrast is lost, appear darker in the image. The O and Ti relative concentration maps are shown in Fig. 6(b) and (c), respectively. The layer is not homogeneous in the lateral length scale, as these maps show an intense decrease of the O concentration in these damaged nano-regions. In Fig. 6(d), we show the calculated Ti oxidation state from the MLLS analysis of Ti $L_{2,3}$ edge. As already shown by the EELS line-scans, within the most damaged O deficient areas the oxidation state is close to +3. As we go deeper in the bulk, over 10 nm far from the surface, the oxidation state reaches a value close to +3.9 but it does not achieve the full +4 value of the bulk (perhaps as an effect of the ion mill induced surface amorphous layer).

4. Discussion

The irradiation of STO single crystals with Ar^+ plasma during reactive ion etching generates a highly damaged area within 10–12 nm of the surface. A clear correlation between the metallic behavior and the surface state of the samples has been observed, the most damaged samples being the ones that present lower resistance values. The irradiation produces a heavy amorphization of the surface, along with significant displacements of the light O atoms, which results in a highly O deficient layer. These damaged regions show a dramatic reduction of Ti atoms, with oxidation states near +3 at the very top layers. Within 10 nm of the surface, approximately, the high structural quality is recovered and the Ti/O ratio values approach those of the bulk. Nevertheless, the Ti ions remain slightly reduced.

From these results we can explain the conduction properties of the STO single crystals, and we find that the electron doping ensuing from the O vacancies is directly responsible for the metallic behavior. Every oxygen vacancy acts as an n-type impurity, releasing two electrons to the lattice. This excess of electrons can be trapped within the Ti 3*d* band, reducing the Ti oxidation state from +4 (with an electronic configuration $3d^0$) to +3 ($3d^1$configuration). Such reduction is responsible for the measured insulator-to-metal transition. It is important to note that the thickness of the conducting layer exceeds the ion range by orders of magnitude, probably due to thermal diffusion of oxygen vacancies into the bulk [16] or to electrons delocalized over long distance due to screening ensuing from the large dielectric constant [33].

5. Conclusions

An unexpected metallic state can be induced on the surface of STO single crystals by means of Ar irradiation. The higher the

irradiation dose, the lower the resistance of the metallic state. Surface characterization by AFM shows that the terrace-like characteristic aspect of untreated substrates is destroyed by the irradiation, suggesting a strong modification of surface features. Aberration-corrected STEM–EELS has been used to study the structure, chemistry and electronic properties of these samples. We have found that one of the most important effects of the treatment is the partial amorphization of a 10 nm thick layer at the very surface, along with a reduction of the O content. The STO directly underneath this layer exhibits good crystallinity, but O vacancies are still present within the range of our measurements. These vacancies act as n-type dopants and reduce the Ti atoms nearby. Electrons in the Ti 3*d* bands become mobile, giving rise to the macroscopically observed metallicity. The amount of irradiation induced damage and the ensuing O vacancies can be tuned through the irradiation conditions, providing an alternate path to produce confined two dimensional metallic states in oxide materials.

Acknowledgments

The authors thank Masashi Watanabe for the Digital Micrograph PCA plug-in. Research at ORNL (SJP and MV) was sponsored by the Materials Sciences and Engineering Division of the US Department of Energy (DOE) and also by by ORNL's Shared Research Equipment (ShaRE) User Program, which is sponsored by the Office of Basic Energy Sciences, US Department of Energy. Research at UCM (GSS) was supported by the ERC starting Investigator Award, Grant #239739 STEMOX.

References

[1] J.F. Shooley, W.R. Hosler, M.L. Cohen, Superconductivity in semiconducting $SrTiO_3$, Physical Review Letters 12 (1964) 474–475.
[2] O.L. Tufte, P.W. Chapman, Electron mobility in semiconducting strontium titanate, Physical Review 155 (1967) 796–802.
[3] H.P.R. Frederikse, W.R. Thurbe, W.R. Hosler, Electronic transport in strontium titanate, Physical Review 134 (1964) A442–A445.
[4] A. Ohtomo, H.Y. Hwang, A high-mobility electron gas at the $LaAlO_3/SrTiO_3$ heterointerface, Nature 427 (2004) 423–426.
[5] G. Herranz, M. Basletic, M. Bibes, C. Carretero, E. Tafra, E. Jacquet, K. Bouzehouane, C. Deranlot, A. Hamzic, J.M. Broto, A. Barthelemy, A. Fert, High mobility in $LaAlO_3/SrTiO_3$ heterostructures: origin, dimensionality, and perspectives, Physical Review Letters 98 (2007) 216803.
[6] A. Kalabukhov, R. Gunnarsson, J. Borjesson, E. Olsson, T. Claeson, D. Winkler, Effect of oxygen vacancies in the $SrTiO_3$substrate on the electrical properties of the $LaAlO_3/SrTiO_3$ interface, Physical Review B 75 (2007) 121404 (R).
[7] P.R. Willmott, S.A. Pauli, R. Herger, C.M. Schleputz, D. Martoccia, B.D. Patterson, B. Delley, R. Clarke, D. Kumah, C. Cionca, Y. Yacoby, Structural basis for the conducting interface between $LaAlO_3$ and $SrTiO_3$, Physical Review Letters 99 (2007) 155502.
[8] S.A. Chambers, Understanding the mechanism of conductivity at the $LaAlO_3/SrTiO_3$(001) interface, Surface Science 605 (2011) 13–14.
[9] K. Yoshimatsu, R. Yasuhara, H. Kumigashira, M. Oshima, Origin of metallic states at the heterointerface between the band insulators $LaAlO_3$ and $SrTiO_3$, Physical Review Letters 101 (2008) 026802.
[10] S.A. Chambers, Comment on "Origin of metallic states at the heterointerface between the band insulators $LaAlO_3$ and $SrTiO_3$", Physical Review Letters 102 (2009) 199703.
[11] F.Y. Bruno, J. Tornos, M. Gutierrez del Olmo, G. Sanchez Santolino, N. Nemes, M. Garcia-Hernandez, B. Mendez, J. Piqueras, G. Antorrena, L. Morellón, J. De Teresa, M. Clement, E. Iborra, C. Leon, J. Santamaria, Anisotropic magneto-transport in $SrTiO_3$ surface electron gases generated by Ar^+ irradiation, Physical Review B 83 (2011) 245120.
[12] D.W. Reagor, V.Y. Butko, Highly conductive nanolayers on strontium titanate produced by preferential ion-beam etching, Nature Materials 4 (2005) 593–596.
[13] V.Y. Butko, H. Wang, D. Reagor, A magnetic field sensitive interfacial metallic state in a crystalline insulator, Nanotechnology 19 (2008) 305401.
[14] D. Kan, T. Terashima, R. Kanda, A. Masuno, K. Tanaka, S. Chu, H. Kan, A. Ishizumi, Y. Kanemitsu, Y. Shimakawa, M. Takano, Blue-light emission at room temperature from Ar^+-irradiated $SrTiO_3$, Nature Materials 4 (2005) 816–819.
[15] D. Kan, R. Kanda, Y. Kan:mitsu, Y. Shimakawa, M. Takano, T. Terashima, A. Ishizumi, Blue luminescence from electron-doped $SrTiO_3$, Applied Physics Letters 88 (2006) 191916.
[16] H. Gross, N. Bansal, Y.S. Kimg, S. Oh, Metal–insulator transition on $SrTiO_3$ surface induced by ionic-bombardment, Journal of Applied Physics 110 (2011) 73704.
[17] G. Koster, B.L. Kropman, G.J.H.M. Rijnders, D.H.A. Blank, H. Rogalla, Quasi-ideal strontium titanate crystal surfaces through formation of strontium hydroxide, Applied Physics Letters 73 (1998) 2920.
[18] L.J. Van der Pauw, A method of measuring specific resistivity and Hall effect of discs of arbitrary shape, Philips Research Reports 13 (1958) 1–9.
[19] O.L. Krivanek, G.J. Corbin, N. Dellby, B.F. Elston, R.J. Keyse, M.F. Murfitt, C.S. Own, Z.S. Szilagyi, J.W. Woodruff, An electron microscope for the aberration-corrected era, Ultramicroscopy 108 (2008) 179–195.
[20] Y. Tokura, Y. Taguchi, Y. Okada, Y. Fujishima, T. Arima, K. Kumagai, Y. Iye, Filling dependence of electronic properties on the verge of metal–Mott–insulator transition in $Sr_{1-x}La_xTiO_3$, Physical Review Letters 70 (1993) 2126–2129.
[21] R. Cowley, The phase transition of strontium titanate, Philosophical Transactions of the Royal Society of London, Series A: Mathematical, Physical and Engineering Sciences 354 (1720) (1996) 2799–2814.
[22] A. Meldrum, L.A. Boatner, W.J. Weber, R.C. Ewing, Amorphization and recrystallization of the ABO_3 oxides, Journal of Nuclear Materials 300 (2002) 242–254.
[23] Y. Zhang, J. Lian, Z. Zhu, W.D. Bennett, L.V. Saraf, J.L. Rausch, C.A. Hendricks, R.C. Ewing, W.J. Weber, Response of strontium titanate to ion and electron irradiation, Journal of Nuclear Materials 389 (2009) 303–310.
[24] M. Varela, M.P. Oxley, W. Luo, J. Tao, M. Watanabe, A.R. Lupini, S.T. Pantelides, S.J. Pennycook, Atomic-resolution imaging of oxidation states in manganites, Physical Review B 79 (2009) 085117.
[25] D.W. Fisher, Molecular-orbital interpretation of the soft X-Ray L II,III emission and absorption spectra from some titanium and vanadium compounds, Journal of Applied Physics 41 (1970) 3561–3569.
[26] L.A. Grunes, R.D. Leapman, C.N. Wilker, R. Hoffman, A.B. Kunz, Oxygen K near-edge fine structure: an electron-energy-loss investigation with comparisons to new theory for selected 3d transition-metal oxides, Physical Review B 25 (12) (1982) 7157.
[27] F.M.F. de Groot, M. Grioni, J.C. Fuggle, Oxygen 1*s* x-ray-absorption edges of transition-metal oxides, Physical Review B 40 (1989) 5715–5723.
[28] H. Kurata, C. Colliex, Electron-energy-loss core-edge structures in manganese oxides, Physical Review B 48 (1993) 2102–2108.
[29] M. Yoshiya, I. Tanaka, K. Kaneko, H. Adachi, First principles calculation of chemical shifts in ELNES/NEXAFS of titanium oxides, Journal of Physics: Condensed Matter 11 (1999) 3217.
[30] E. Stoyanov, F. Langenhorst, G. Steinle-Neumann, The effect of valence state and site geometry on Ti $L_{3,2}$ and O *K* electron energy-loss spectra of Ti_xO_y phases, American Mineralogist 92 (2007) 577–586.
[31] S.D. Berger, S.J. Pennycook, Detection of nitrogen at (100) platelets in diamond, Nature 298 (1982) 635–637.
[32] J. Garcia-Barriocanal, F.Y. Bruno, A. Rivera-Calzada, Z. Sefrioui, N.M. Nemes, M. Garcia-Hernández, J. Rubio-Zuazo, G.R. Castro, M. Varela, S.J. Pennycook, C. Leon, J. Santamaria, "Charge Leakage" at $LaMnO_3/SrTiO_3$ interfaces, Advanced Materials 22 (2010) 627–632.
[33] J.H. Ngai, Y. Segal, D. Su, Y. Zhu, F.J. Walker, S. Ismail-Beigi, K. LeHur, C.H. Ahn, Electric field tuned crossover from classical to weakly localized quantum transport in electron doped $SrTiO_3$, Physical Review B 81 (2010) 241307 (R).